New Developments on Metallurgy and Applications of High Strength Steels, Buenos Aires 2008, Argentina

Complete Calculation of Steel Microstructure for Strong Alloys

J. Chen, H. K. D. H. Bhadeshia, †S. Hasler, †H. Roelofs and †U. Ulrau

University of Cambridge
Materials Science and Metallurgy, Cambridge CB2 3QZ, U. K.

†Swiss Steel AG, Emmenbrücke, Switzerland

Keywords: Mathematical model, phase transformations, microstructure

Abstract

Strong steels also have to be tough and hence rely on fine microstructures such as bainite or martensite, produced commercially by continuous cooling transformation. Depending on the detailed requirements, the steel-design process may explicitly require other higher temperature phases to be absent in the final microstructure. Such a procedure can be made easier by the availability of a good method for calculating the transformation characteristics of a steel as a function of its chemical composition, austenite grain structure and cooling conditions.

We present here a method for doing so using simultaneous transformation theory and mechanistic models for allotriomorphic and idiomorphic ferrite, Widmanstätten ferrite, pearlite, bainite, martensite and retained austenite. All of these details including thermodynamic and kinetic definitions of each of the phases have been incorporated into a computer algorithm which seems to correctly reproduce the trends expected from physical metallurgy principles, but on a firm quantitative basis.

1 Introduction

There has been a great deal of research published on the development of microstructure due to the solid–state transformation of austenite in steels. Much of this has dealt with the mechanism, thermodynamics and kinetics of individual transformation products such as allotriomorphic ferrite, Widmanstätten ferrite, pearlite, bainite and martensite; there have also been a few attempts at integrating all of these transformations into unified schemes which lead to the calculation of continuous cooling transformation characteristics as a function of steel composition and thermomechanical processing [1–5]. There are varying degrees of empiricism and none of these models have a simultaneous transformation framework. The essence of such a framework is to allow all

transformations to occur at the same time at all temperatures; whether a transformation actually occurs depends on the available driving force and kinetics in the context of the mechanism of the transformation concerned. In this way, artificial rules as to when a transformation can begin and stop are avoided.

The first application of the simultaneous transformation framework came in the context of power plant steels [6–8] and structural steels [9, 10]. It is the latter case which is of interest here because [10] because it dealt with steels containing ferrite, Widmanstätten ferrite and pearlite. Bainite and martensite could not at that time be incorporated into the framework, but recent work has led to a mechanistic model for bainite [11–13]. The purpose of the work presented here was to integrate the bainite model into the framework; this would in the future permit the integration of other theory [14] for martensite and any retained austenite at the point the steel cools to room temperature.

The intention was to create a comprehensive model dealing with allotriomorphic ferrite [15], Widmanstätten ferrite [16], pearlite [17] and carbide–free bainite [11], as a function of the steel chemical composition (C, Mn, Si, Ni, Mo, Cr, V), the austenite grain size [18] and cooling conditions. The detailed mechanisms of transformation for each of these phases are described in the references quoted and a summary is available in Table 15.1 of [19].

We describe here the broad algorithms used to do the calculations which are all based on nucleation, growth and overall transformation kinetics [20–22].

2 Algorithm

The sequence of calculation is illustrated in Fig. 1, beginning with information of the chemical composition of the steel with respect to common solutes, the austenite grain size and the proposed heat treatment, whether this is continuous cooling or isothermal transformation.

The chemical composition is then used to calculate the thermodynamics of transformation from austenite [23–26], including the free energy changes $\Delta G^{\gamma\rightarrow\alpha+\gamma'}$, $\Delta G^{\gamma\rightarrow\alpha}$, and ΔG_m as illustrated in Fig. 6.2 of [19] and the phase compositions. The method assumes paraequilibrium transformation. Diffusion coefficients are calculated as in [27–29]. These data were then used to calculated the nucleation and growth kinetics assuming the mechanisms outlined in Table 1, and in detail in [15, 26, 30].

3 Overall Transformation Kinetics

Once nucleation and growth functions are established, it is necessary to deal with overall transformation kinetics, *i.e.,* the evolution of the fraction of transformation, hard–impingement between particles growing from different locations and soft–impingement due to the overlap of the diffusion fields of particles growing from different locations. This can be done using Avrami theory [32–35].

Table 1: The assumed atomic mechanisms of phase transformation from austenite [30]. Paraequilibrium is a state in which carbon achieves a uniform chemical potential subject to the constraint that the substitutional solute to iron atom ratio remains constant [15, 31].

Phase	Atomic mechanism	Nucleation	Growth
Allotriomorphic ferrite	Reconstructive	Paraequilibrium	Paraequilibrium
Pearlite	Reconstructive	Paraequilibrium	Paraequilibrium
Widmanstätten ferrite	Displacive	Paraequilibrium	Paraequilibrium
Bainite	Displacive	Paraequilibrium	Diffusionless
Martensite	Displacive	Diffusionless	Diffusionless

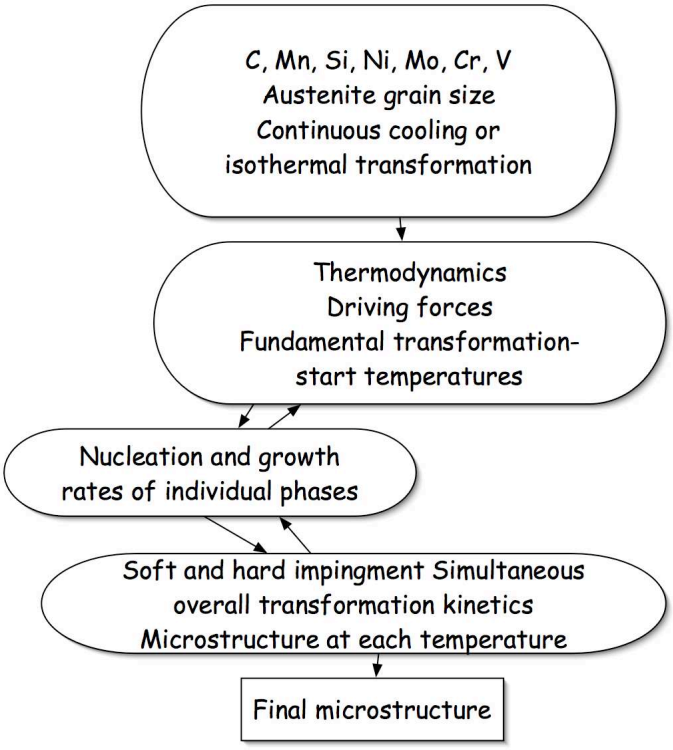

Figure 1: Architecture of the algorithm used to calculate the evolution of microstructure

Referring to Fig. 2, suppose that two particles exist at time t; a small interval δt later, new regions marked a, b, c & d are formed assuming that they are able to grow unrestricted in extended space whether or not the region into which they grow is already transformed. However, only those components of a, b, c & d which lie in previously untransformed matrix can contribute to a change in the real volume of the product phase (α) :

$$dV^{\alpha} = \left(1 - \frac{V^{\alpha}}{V}\right) dV_e^{\alpha} \tag{1}$$

where it is assumed that the microstructure develops at random. The subscript e refers to extended volume, V^{α} is the volume of α and V is the total volume. Multiplying the change in extended volume by the probability of finding untransformed regions has the effect of excluding regions such as b, which clearly cannot contribute to the real change in volume of the product. For a random distribution of precipitated particles, this equation can easily be integrated to obtain the real volume fraction,

$$\frac{V^{\alpha}}{V} = 1 - \exp\left\{-\frac{V_e^{\alpha}}{V}\right\} \tag{2}$$

The extended volume V_e^{α} is straightforward to calculate using nucleation and growth models and neglecting completely any impingement effects.

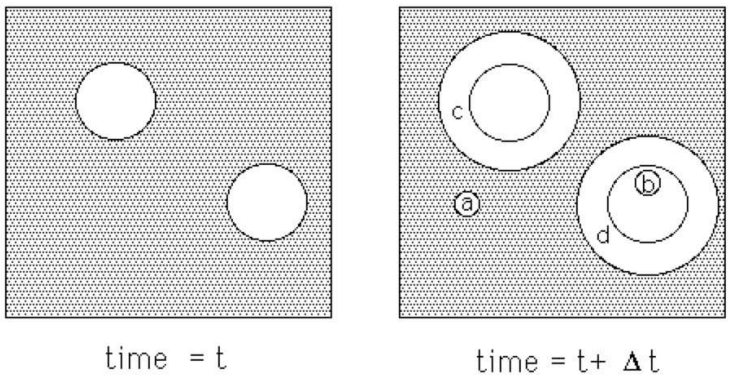

Figure 2: Concept of extended volume. New regions c and d are formed in the interval Δt as the original particles grow, and new particles a and b nucleate.

Multiple reactions occurring simultaneously can be accounted for by forming coupled equations [6–10]; thus for two phases:

$$dV^{\alpha} = \left(1 - \frac{V^{\alpha} + V^{\beta}}{V}\right) dV_e^{\alpha} \qquad \text{and} \qquad dV^{\beta} = \left(1 - \frac{V^{\alpha} + V^{\beta}}{V}\right) dV_e^{\beta} \tag{3}$$

This can be done for any number of reactions and when solved numerically, has the advantage of permitting the boundary conditions to be altered to account for a change in the average composition of the matrix (mean field approximation to account for soft impingement).

4 Numerical Scheme

To model the gradual development of microstructure the calculation is divided into time steps which lead to an appropriate numerical accuracy. During one time step, the increase in extended

volume of phase i at time τ is written $\Delta V^e_{i,\tau}$. The real change in volume, $\Delta V_{i,\tau}$ is then:

$$\Delta V_{i,\tau} = \Delta V^e_{i,\tau}\left(1 - \frac{\sum V_{i,\tau}}{V_{tot}}\right) \tag{4}$$

where $V_{i,\tau}$ is the total transformed volume of phase i at time τ and V_{tot} is the total volume of the system.

Since many reactions are nucleated at grain boundaries rather than at random locations, we use the adaptation to the extended space concept by Cahn [36] to deal with such reactions. Impingement then occurs in two forms, along the grain boundary plane (dealt with the extended area concept) and between particles originating from different boundaries (dealt with the extended volume concept). The details have been described elsewhere [9, 10].

5 Bainite

The work published by Jones and Bhadeshia [9, 10] dealt with allotriomorphic, idiomorphic and Widmanstätten ferrite and pearlite, but not with bainite. This has to await development of a rigourous model for the transformation [11], which we have now integrated into the overall scheme to produce a more comprehensive treatment of solid–state transformations in steels.

There are complications because bainite grows in the form of sheaves made up of small sub–units (Fig. 3). The growth process of a sheaf is the successive nucleation of sub-units on the tips of the previous ones. It takes a longer time to nucleate the next sub-unit on the tip of the current one than to grow a sub-unit itself. Therefore the growth rate is determined by the nucleation time or the incubation time between two successive sub-units.

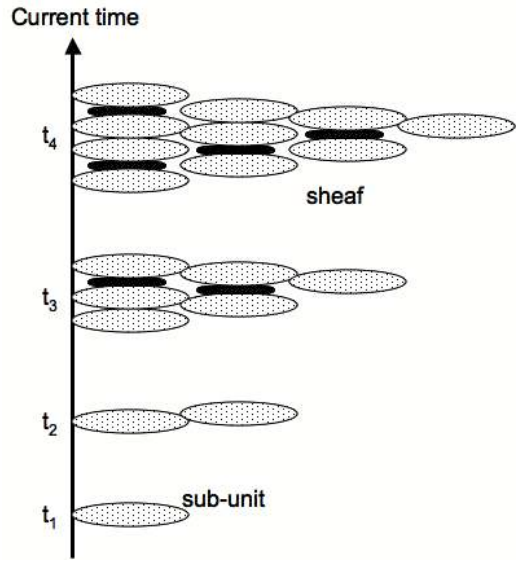

Figure 3: Bainite sheaves are composed of smaller platelets. The sheaf evolves by the successive nucleation of sub–units as illustrated.

The overall growth rate of a sheaf is substantially less than that of a sub–unit, so that there is an incubation time where the sheaf is salient before it next propagates. A sheaf is allowed to grow

if the time interval since it last grew is greater than the incubation time (Fig. 4). This test is conducted for each sheaf, so that some of the sheaves may growth and others have to wait until the condition is satisfied.

The nucleation of a sheaf begins with that of the first sub–unit at an austenite grain boundary as illustrated in Fig. 3. It follows from the procedure described in the last paragraph that sheaves initiated at the same point in time will evolve in an exactly identical manner as time progresses. It is necessary therefore in the algorithm to group together the sheaves which initiated at a particular point in time.

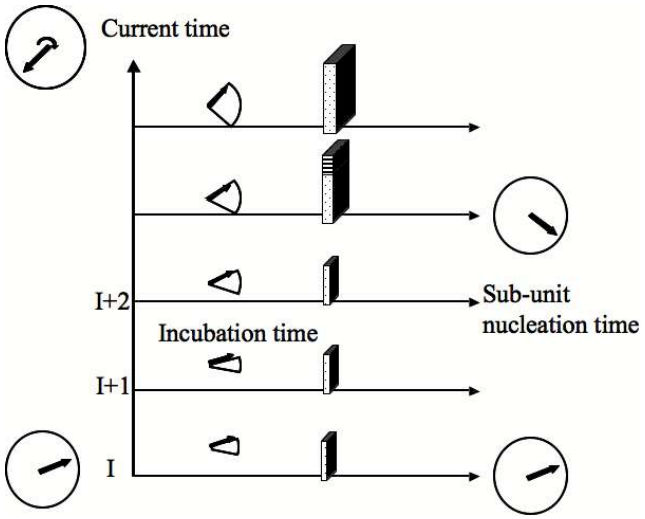

Figure 4: Illustrating the intermittent growth of a sheaf. If the waiting time since its last growth step is greater than the incubation time, then growth is resumed, and *vice versa*.

6 Implementation

The computer program used here has been developed over decades of research and large parts of it have been validated through a variety of experiments and theoretical assessments. However, the ability to rigourously handle many transformations at the same time is relatively recent [9, 10], and that component was originally validated by comparing against the experimental data of Bodnar and Hansen [37] for a steel of composition Fe–0.18C–0.18Si–1.15Mn–0.003V wt% for a variety of austenite grain sizes and cooling rates (Table 2). The level of agreement between theory and experiment found in that work [9, 10] is illustrated in Fig. 5a. Although the agreement was considered at the time to be reasonable, there clearly are discrepancies and the data are not uniformly distributed about the line of perfect consistency between experiment and theory. Better agreement has been achieved in the present work after removing some errors in the original computer program, Fig. 5b.

The bainite part of the program is completely new, and after integration the nucleation parameters were set by testing against the isothermal carbide–free bainite experimental data of [38] for Fe–0.44C–1.74Si–0.67Mn–1.85Ni–0.83Mo–0.39Cr–0.09V wt% and an austenite grain size of 86 μm. These data were used to derive the fitting parameters for the bainite part of the program. As a result, the reasonable agreement obtained in Fig. 6 is not surprising, but it is good that the model

Austenite grain size / μm	30	30	30	30	30	55	55	55
Cooling rate / K min^{-1}	101	59	30	16	11	99	59	30
Austenite grain size μm	55	55	100	100	100	100	100	
Cooling rate / K min^{-1}	16	11	101	59	30	16	11	

Table 2: The details of the experiments by Bodnar and Hansen [37].

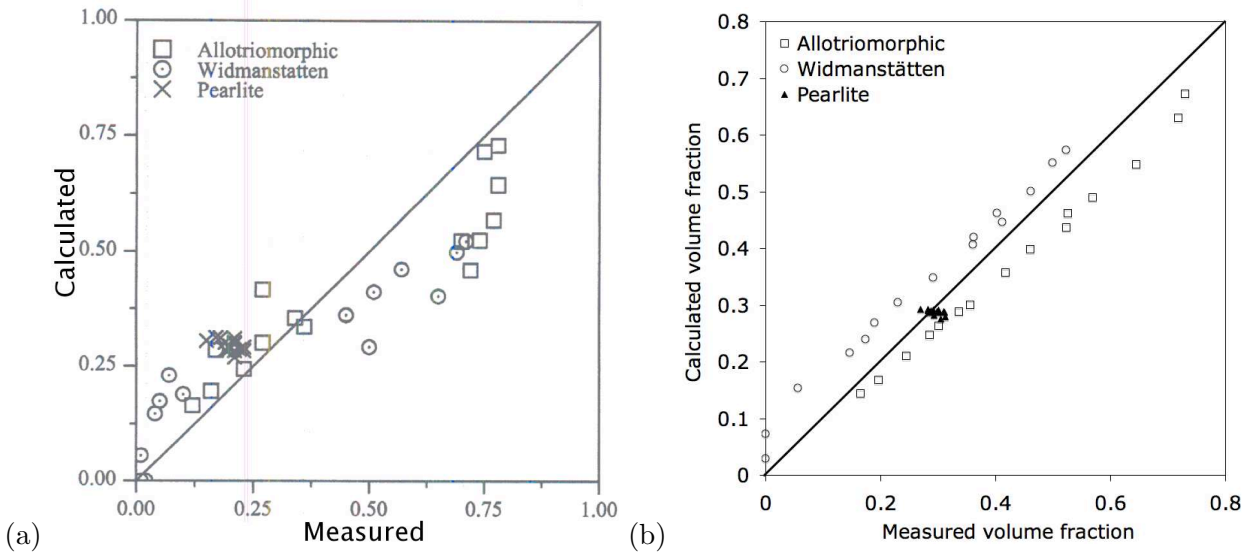

Figure 5: (a) Comparison of calculated and measured fractions Bodnar:1994 for the original work by Jones and Bhadeshia [9]. (b) Comparison of calculations done using the modified program from the present work, with the Bodnar and Hansen data.

has captured the incomplete reaction phenomenon [19, 39] accurately. In this, the extent of reaction decreases at the transformation temperature is increased.

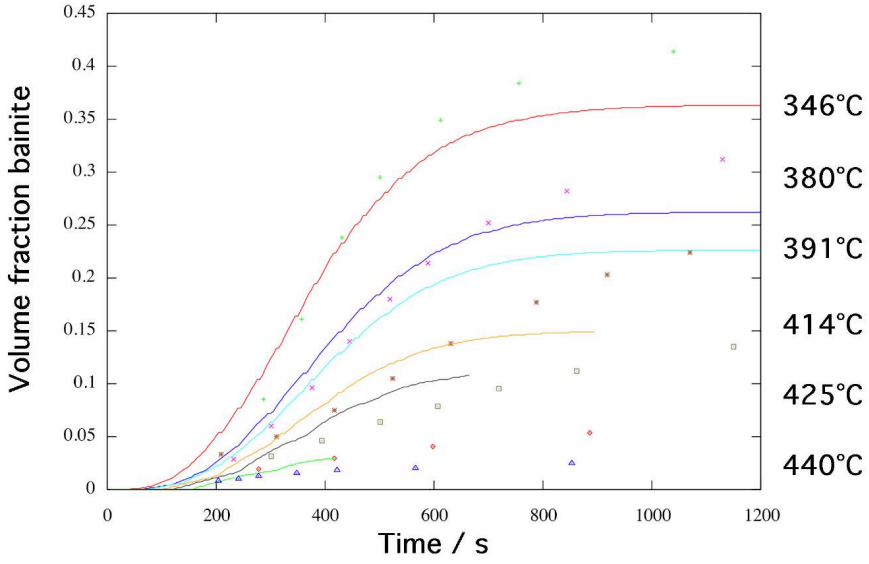

Figure 6: Comparison of experimental measurements [38] of the fraction of carbide–free bainite as a function of the isothermal transformation temperature, against computations (curves).

7 Summary

It has been possible for the first time to integrate the bainite reaction into the simultaneous transformations framework so that allotriomorphic ferrite, Widmanstätten ferrite, pearlite and bainite can be calculated without putting artificial constraints on where transformations should start and finish. The work requires greater validation and although some results will be reported in our companion paper, attempts are underway to compare the computations against published atlases of continuous cooling transformation diagrams.

Acknowledgements

We are grateful to Swiss Steel for financing this work and to Professor A. L. Greer for the provision of laboratory facilities at the University of Cambridge.

References

[1] J. S. Kirkaldy, B. A. Thomson, and E. Baganis. Prediction of multicomponent equilibrium and transformation diagrams for low alloy steels. In D. V. Doane and J. S. Kirkaldy, editors, *Hardenability concepts with applications to steels*, pages 82–125, Materials Park, Ohio, USA, 1978. TMS–AIME.

[2] M. Umemoto and I. Tamura. Computer simulation of isothermal transforamtion diagrams for steels. *Bulletin of the Japan Institute of Metals*, 22:497–504, 1985.

[3] H. K. D. H. Bhadeshia, L.-E. Svensson, and B. Gretoft. Model for the development of microstructure in low alloy steel (Fe-Mn-Si-C) weld deposits. *Acta Metallurgica*, 33:1271–1283, 1985.

[4] P. J. van der Wolk, J. J. Wang, J. Seitsma, and S. van der Zwaag. Modelling the continuous cooling transformation diagram of engineering steels using neural networks - part i: Phase regions. *Zeitschrift fur Metallkunde*, 93:1199–1207, 2002.

[5] T. Trzaska and L. A. Dobrzanski. Modelling of cct diagrams for engineering and constructional steels. *Journal of Materials Processing Technology*, 192:504–510, 2007.

[6] J. D. Robson and H. K. D. H. Bhadeshia. Kinetics of precipitation in power plant steels. *CALPHAD*, 20:447–460, 1996.

[7] J. D. Robson and H. K. D. H. Bhadeshia. Modelling precipitation sequences in power plant steels: Part i, kinetic theory. *Materials Science and Technology*, 13:631–639, 1997.

[8] J. D. Robson and H. K. D. H. Bhadeshia. Modelling precipitation sequences in power plant steels, part 2: Application of kinetic theory. *Materials Science and Technology*, 28A:640–644, 1997.

[9] S. Jones and H. K. D. H. Bhadeshia. Competitive formation of inter- and intragranularly nucleated ferrite. *Metallurgical & Materials Transactions A*, 28A:2005–2103, 1997.

[10] S. Jones and H. K. D. H. Bhadeshia. Kinetics of the simultaneous decomposition of austenite into several transformation products. *Acta Materialia*, 45:2911–2920, 1997.

[11] H. Matsuda and H. K. D. H. Bhadeshia. Kinetics of the bainite transformations. *Proceedings of the Royal Society of London A*, A460:1710–1722, 2004.

[12] G. I. Rees and H. K. D. H. Bhadeshia. Bainite transformation kinetics, part i, modified model. *Materials Science and Technology*, 8:985–993, 1992.

[13] G. I. Rees and H. K. D. H. Bhadeshia. Bainite transformation kinetics, part ii, non-uniform distribution of carbon. *Materials Science and Technology*, 8:994–996, 1992.

[14] P. Koistinen D and R. E. Marburger. A general equation prescribing the extent of the austenite-martensite transformation in pure iron–carbon alloys and plain carbon steels. *Acta Metallurgica*, 7:59–60, 1959.

[15] H. K. D. H. Bhadeshia. Diffusional formation of ferrite in iron and its alloys. *Progress in Materials Science*, 29:321–386, 1985.

[16] H. K. D. H. Bhadeshia. Critical assessment: Diffusion–controlled growth of ferrite plates in plain carbon steels. *Materials Science and Technology*, 1:497–504, 1985.

[17] M. Takahashi. *Reaustenitisation from bainite in steels*. PhD thesis, University of Cambridge, 1992.

[18] Q. Zhu, C. M. Sellars, and H. K. D. H. Bhadeshia. Quantitative metallography of deformed grains. *Submitted to Materials Science and Technology*, 2006.

[19] H. K. D. H. Bhadeshia. *Bainite in Steels, 2nd edition*. Institute of Materials, London, 2001.

[20] H. K. D. H. Bhadeshia and A. L. Greer. *Introduction ot Materials Modelling*, chapter 5. Maney, London, 2005.

[21] J. W. Christian. *Theory of Transformations in Metal and Alloys, Part II*. Pergamon Press, 3 edition, 2003.

[22] J. W. Christian. *Theory of Transformations in Metal and Alloys, Part I*. Pergamon Press, Oxford, U. K., 3 edition, 2003.

[23] H. I. Aaronson, H. A. Domian, and G. M. Pound. Thermodynamics of the austenite - poreutectoid ferrite transformation I, Fe-C alloys. *TMS–AIME*, 236:753–767, 1966.

[24] H. I. Aaronson, H. A. Domian, and G. M. Pound. Thermodynamics of the austenite - poreutectoid ferrite transformation II, Fe–C–X alloys. *TMS–AIME*, 236:768–780, 1966.

[25] H. I. Aaronson, H. A. Domian, and G. M. Pound. Partitioning of alloying elements between austenite and proeutectoid ferrite and bainite. *TMS–AIME*, 236:781–796, 1966.

[26] H. K. D. H. Bhadeshia. Rationalisation of shear transformations in steels. *Acta Metallurgica*, 29:1117–1130, 1981.

[27] R. H. Siller and R. B. McLellan. The variation with composition of the diffusivity of carbon in austenite. *TMS–AIME*, 245:697–700, 1969.

[28] S. S. Babu and H. K. D. H. Bhadeshia. Diffusion of carbon in substitutionally alloyed austenite. *Journal of Materials Science Letters*, 14:314–316, 1985.

[29] H. K. D. H. Bhadeshia. Diffusion of carbon in austenite. *Metal Science*, 15:477–479, 1981.

[30] H. K. D. H. Bhadeshia and J. W. Christian. The bainite transformation in steels. *Metallurgical & Materials Transactions A*, 21A:767–797, 1990.

[31] M. Hillert. Använding av isoaktiva linjer i ternära till–ståndS–diagram. *Jernkontorets Annaler*, 136:25–37, 1952.

[32] M. Avrami. Kinetics of phase change 1. *Journal of Chemical Physics*, 7:1103–1112, 1939.

[33] M. Avrami. Kinetics of phase change 2. *Journal of Chemical Physics*, 8:212–224, 1940.

[34] M. Avrami. Kinetics of phase change 3. *Journal of Chemical Physics*, 9:177–184, 1941.

[35] W. A. Johnson and R. F. Mehl. Reaction kinetics in processes of nucleation and growth. *TMS–AIMME*, 135:416–458, 1939.

[36] J. W. Cahn. The kinetics of grain boundary nucleated reactions. *Acta Metallurgica*, 4:449–459, 1956.

[37] R. L. Bodnar and S. S. Hansen. Effects of austenite grain size and cooling rate on Widmanstätten ferrite formation in low alloy steels. *Metallurgical & Materials Transactions A*, 25A:665–675, 1994.

[38] H. K. D. H. Bhadeshia. Bainite: Overall transformation kinetics. *Journal de Physique Colloque*, C4 43:443–448, 1982.

[39] P. G. Self, H. K. D. H. Bhadeshia, and W. M. Stobbs. Lattice spacings from lattice fringes. *Ultramicroscopy*, 6:29–40, 1981.